Supporting Information

Metal-Organic Coordination Polymer to Prepare Density Controllable and High Nitrogen Doped Content Carbon/Graphene for High Performance Supercapacitors

Jinwei Luo,[†] Wenbin Zhong,[*,†] Yubo Zou,[†] Changlun Xiong,[†] Wantai Yang[‡]

[†] College of Materials Science and Engineering, Hunan University, Changsha, 410082, P. R. China.

[‡] Department of Polymer Science, Beijing University of Chemical Technology, Beijing, 100029, P. R. China.

*E-mail: wbzhong@hnu.edu.cn

1. Raman spectra analysis of the as-prepared samples.

Table S1. The Raman spectra analysis of NCG_{Cu}, NC_{Cu}, NCG_{Fe}, NC_{Fe}, NCG_{Zn} and NC_{Zn}

Samples	D-Band	G-Band	I_D/I_G [a]
NCG_{Cu}	1333.4	1590.1	1.76
NC_{Cu}	1346.9	1584.2	2.04
NCG_{Fe}	1335.1	1589.2	1.97
NC_{Fe}	1354.5	1585.8	2.05
NCG_{Zn}	1326.7	1587.5	2.07
NC_{Zn}	1343.5	1588.3	2.31

[a] The ratio of I_D/I_G was calculated based on the peak area of D-Band and G-Band.

2. The porosity parameter of the carbon materials.

Table S2. Characteristic surface areas and pore structures of NCG_{Cu}, NCG_{Fe} and NCG_{Zn} without treatment of acid

Samples	BET surface area ($m^2 g^{-1}$)		Total pore volume ($cm^3 g^{-1}$)	Average pore size (nm)
	Total	S_{micro}		
NCG_{Cu} without acid treatment	91.17	19.29	0.232	10.18
NCG_{Fe} without acid treatment	209.0	170.15	0.180	3.45
NCG_{Zn} without acid treatment	405.02	368.52	0.228	2.25

Notes: S_{micro} represents the micropore area.

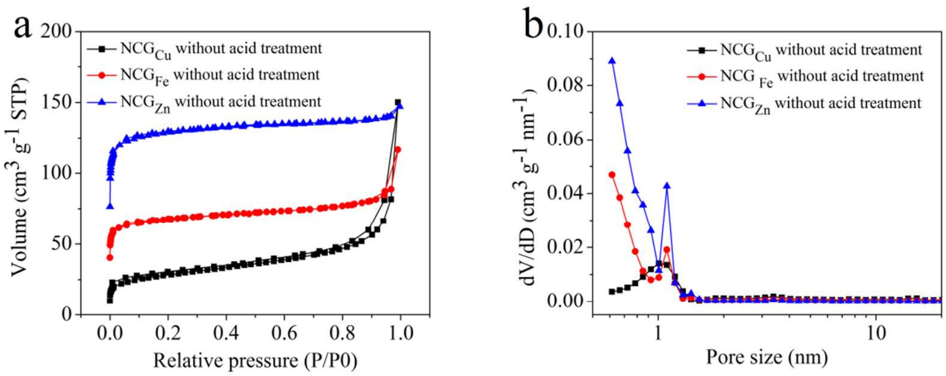

Figure S1. (a) Nitrogen adsorption-desorption isotherms and (b) pore size distribution of NCG_{Cu}, NCG_{Fe} and NCG_{Zn}, which were not washed by acids. (STP = standard temperature and pressure).

3. XPS analysis of the as-prepared samples.

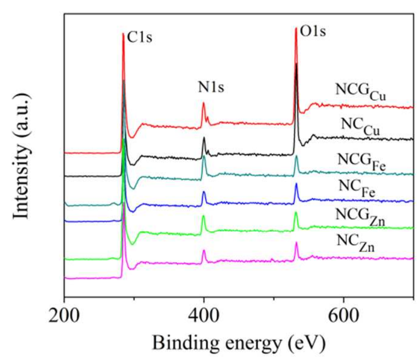

Figure S2. XPS survey of NCG_{Cu}, NC_{Cu}, NCG_{Fe}, NC_{Fe}, NCG_{Zn} and NC_{Zn}.

Table S3. The elemental composition and atomic contents (at.%) of NCG_{Cu}, NC_{Cu}, NCG_{Fe}, NC_{Fe}, NCG_{Zn} and NC_{Zn}

Samples	C	N	O
NCG_{Cu}	68.81	10.68	20.51
NC_{Cu}	65.11	11.72	23.17
NCG_{Fe}	81.43	12.99	5.58
NC_{Fe}	80.41	10.99	8.60
NCG_{Zn}	83.16	11.21	5.63
NC_{Zn}	81.24	10.58	8.18

Table S4. Relative ratio (%) of different nitrogen components in NCG_{Cu}, NC_{Cu}, NCG_{Fe}, NC_{Fe}, NCG_{Zn} and NC_{Zn} from N 1s XPS spectra which were calculated based on the areas of the XPS peaks

Samples	Pyridinic-N (N-6)	Pyrrolic/pyridone-N (N-5)	Quaternary-N (N-Q)	Pyridine-N -oxide (N-X)
Binding energy(eV)	~398.3	~400.0	~401.1	~403.4-405.6
NCG_{Cu}	21.20	41.32	22.03	15.45
NC_{Cu}	26.31	37.58	21.73	14.38
NCG_{Fe}	36.39	27.65	22.13	13.83
NC_{Fe}	37.79	25.94	25.55	12.72
NCG_{Zn}	32.34	29.39	24.44	13.83
NC_{Zn}	33.70	33.07	21.30	11.93

Table S5. Relative ratio (%) of different oxygen components in NCG_{Cu}, NC_{Cu}, NCG_{Fe}, NC_{Fe}, NCG_{Zn} and NC_{Zn} from O 1s XPS spectra which were calculated based on the areas of the XPS peaks

Samples	C=O (O-I)	C-OH, C-O-C (O-II)	COOH (O-III)
Binding energy(eV)	531.0	532.4	533.6
NCG_{Cu}	48.22	35.06	16.72
NC_{Cu}	49.52	33.78	16.70
NCG_{Fe}	37.94	34.49	27.57
NC_{Fe}	45.37	28.71	28.72
NCG_{Zn}	30.16	28.76	41.08
NC_{Zn}	40.54	35.01	24.45

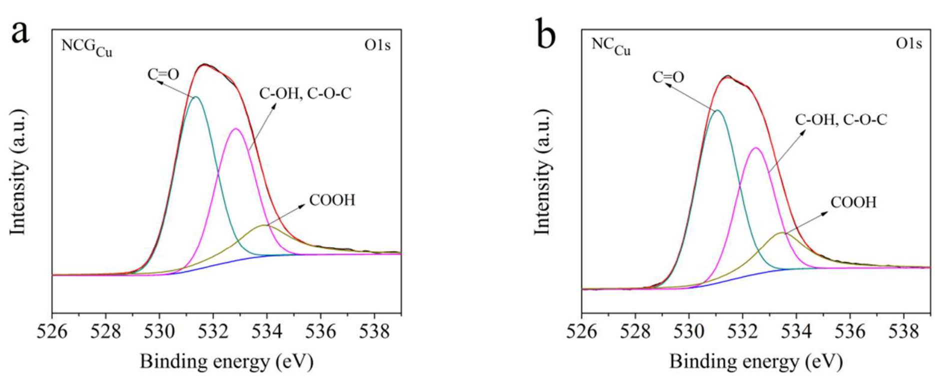

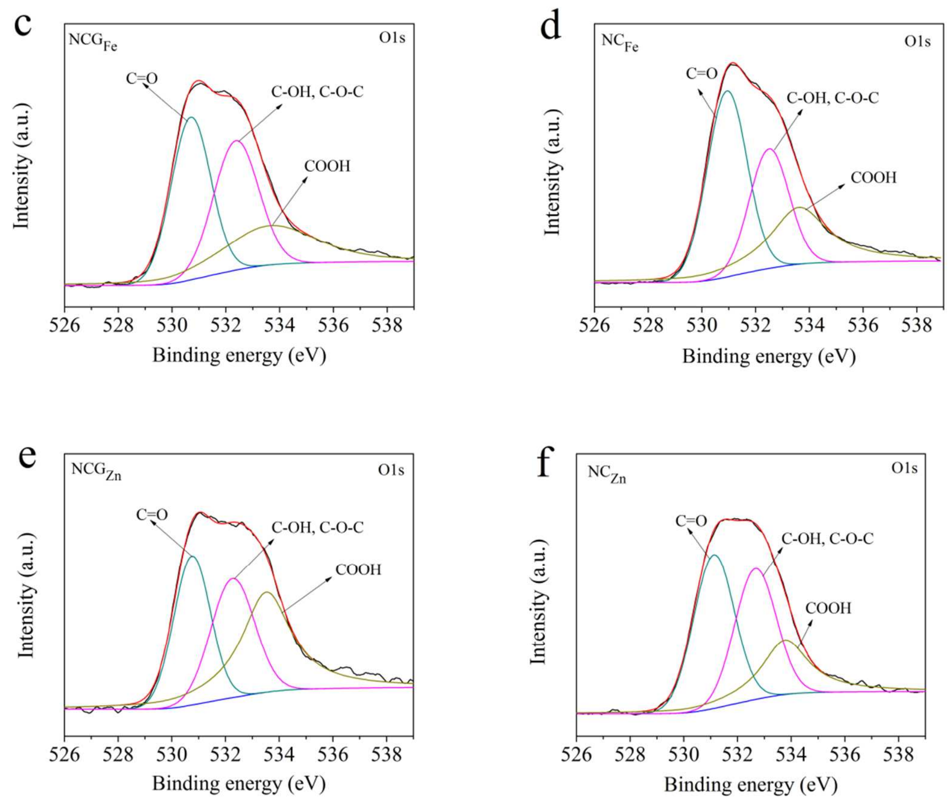

Figure S3. O 1s spectra of (a) NCG_{Cu}, (b) NC_{Cu}, (c) NCG_{Fe}, (d) NC_{Fe}, (e) NCG_{Zn} and (f) NC_{Zn}.

4. Electrochemical characterization of supercapacitors based on NCG_{Cu} and the affect factors, such as the amount of BPD, $CuCl_2$, and pyrolysis temperature, to their electrochemical performances.

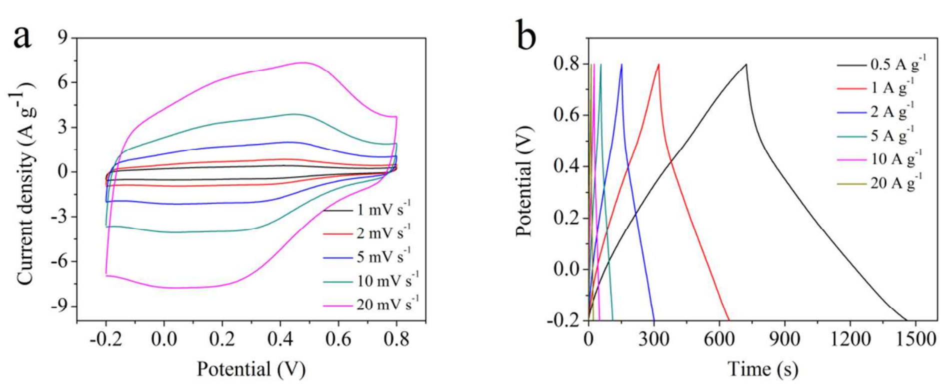

Figure S4. Electrochemical characterization of supercapacitors based on NCG_{Cu} (The mass ratio of GO/BPD was 1:10, the molar ratio of BPD/$CuCl_2$ was 1:0.6, and the pyrolysis temperature was 650℃.): (a) Cyclic voltammetry curves at different scan rates (1-20 mV s^{-1}). (b) Galvanostatic charge/discharge curves at different current densities (0.5-20 A g^{-1}).

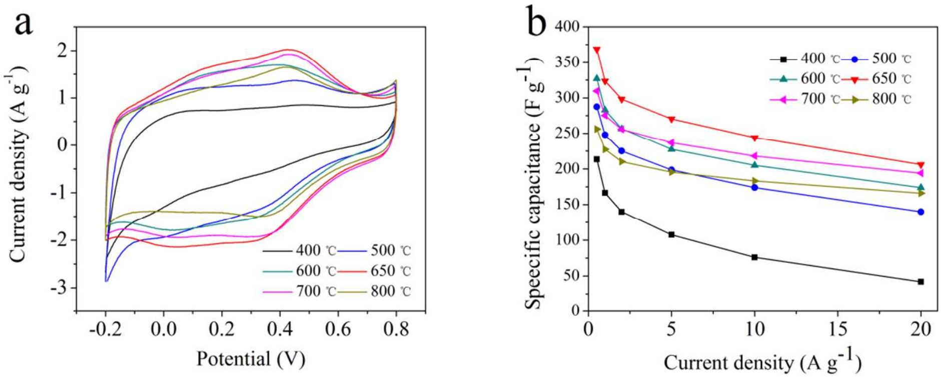

Figure S5. Electrochemical characterization of supercapacitors based on NCG_{Cu} samples with different pyrolysis temperature (400, 500, 600, 650, 700 and 800℃, respectively): (a) Cyclic voltammetry curves at a scan rates of 5 mV s^{-1}. (b) The specific capacitances at different current density ranging from 0.5 to 20 A g^{-1}.

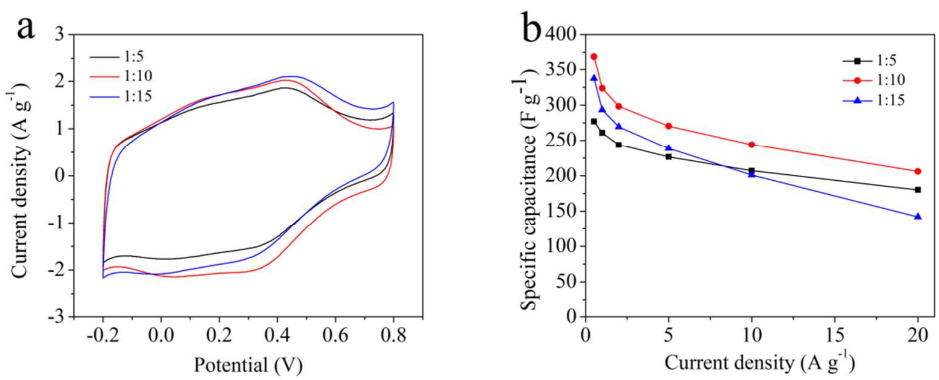

Figure S6. Electrochemical characterization of supercapacitors based on NCG_{Cu} samples with different mass ratio of GO/BPD (1:5, 1:10 and 1:15): (a) Cyclic voltammetry curves at a scan rate of 5 mV s^{-1}. (b) The specific capacitances at different current density ranging from 0.5 to 20 A g^{-1}.

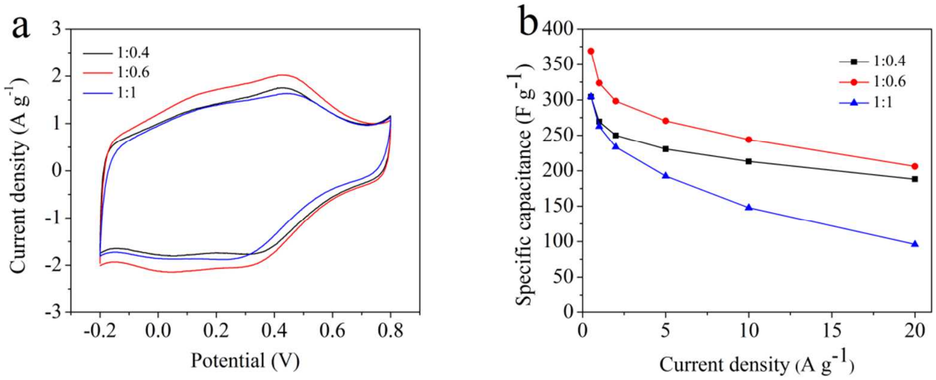

Figure S7. Electrochemical characterization of supercapacitors based on NCG_{Cu} samples with different molar ratio of BPD/$CuCl_2$ (1:0.4, 1:0.6 and 1:1, respectively): (a) Cyclic voltammetry curves at a scan rates of 5 mV s^{-1}. (b) The specific capacitances at different current density ranging from 0.5 to 20 A g^{-1}.

5. Electrochemical characterization of supercapacitors based on NCG_{Fe} and the affect factors (including the amount of BPD, $FeCl_3$, and pyrolysis temperature) to their electrochemical performances.

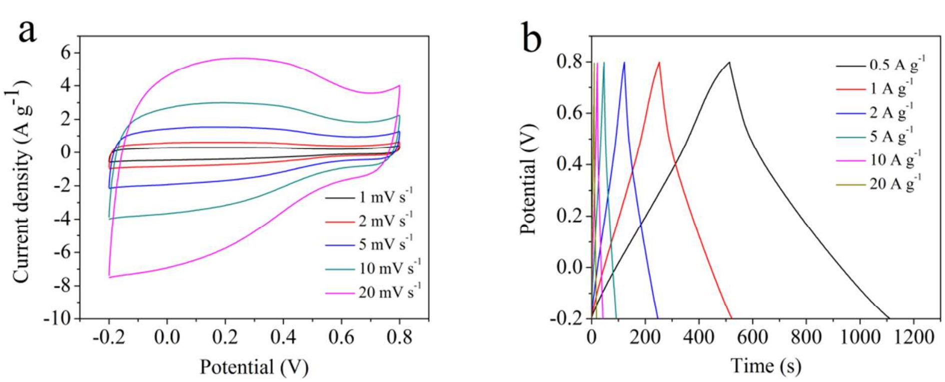

Figure S8. Electrochemical characterization of supercapacitors based on NCG_{Fe} (The mass ratio of GO/BPD was 1:10, the molar ratio of BPD/$FeCl_3$ was 1:0.6, and the pyrolysis temperature was 600℃.): (a) Cyclic voltammetry curves at different scan rates (1-20 mV s^{-1}). (b) Galvanostatic charge/discharge curves at different current densities (0.5-20 A g^{-1}).

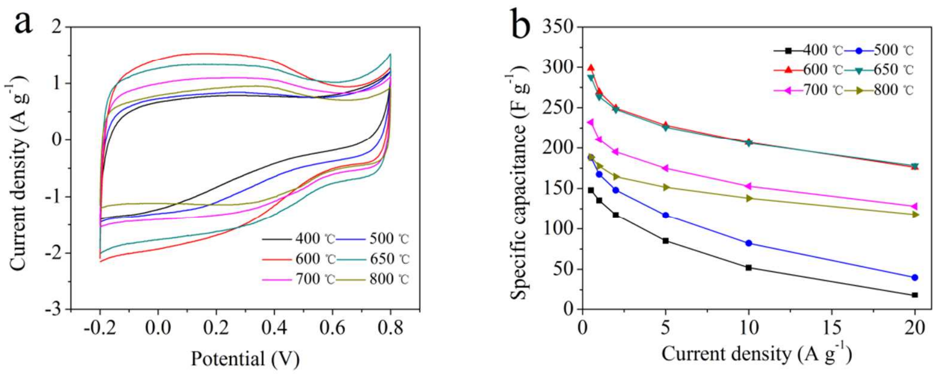

Figure S9. Electrochemical characterization of supercapacitors based on NCG_{Fe} samples with different pyrolysis temperature (400, 500, 600, 650, 700 and 800℃, respectively): (a) Cyclic voltammetry curves at a scan rates of 5 mV s^{-1}. (b) The specific capacitances at different current density ranging from 0.5 to 20 A g^{-1}.

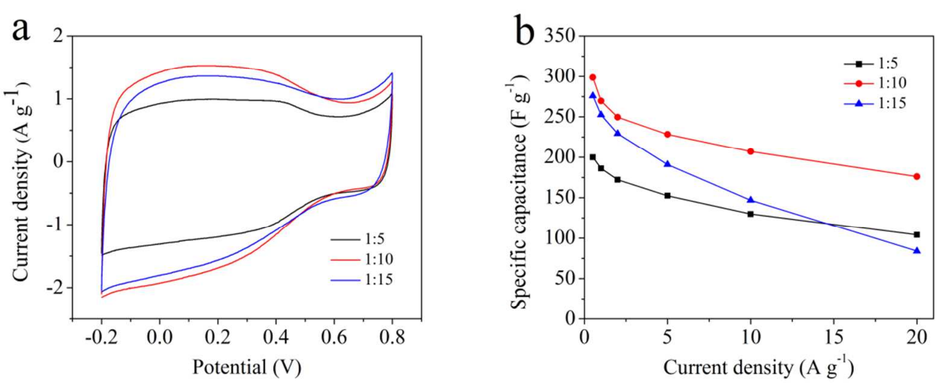

Figure S10. Electrochemical characterization of supercapacitors based on NCG_{Fe} samples with different mass ratio of GO/BPD (1:5, 1:10 and 1:15, respectively): (a) Cyclic voltammetry curves at a scan rates of 5 mV s^{-1}. (b) The specific capacitances at different current density ranging from 0.5 to 20 A g^{-1}.

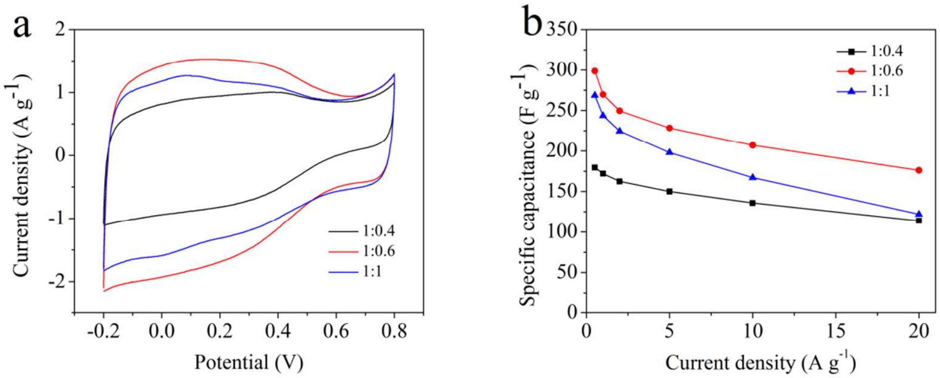

Figure S11. Electrochemical characterization of supercapacitors based on NCG_{Fe} samples with different molar ratio of BPD/$FeCl_3$ (1:0.4, 1:0.6 and 1:1, respectively): (a) Cyclic voltammetry curves at a scan rates of 5 mV s^{-1}. (b) The specific capacitances at different current density ranging from 0.5 to 20 A g^{-1}.

6. Electrochemical characterization of supercapacitors based on NCG_{Zn} and the affect factors (including the amount of BPD, $ZnCl_2$, and pyrolysis temperature) to their electrochemical performances.

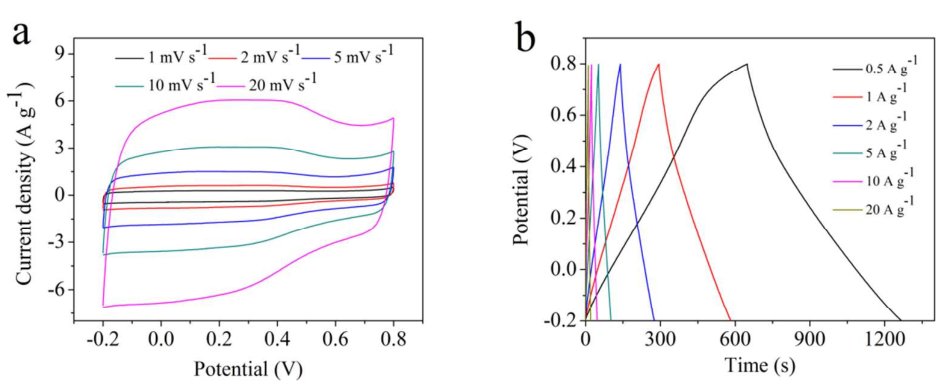

Figure S12. Electrochemical characterization of supercapacitors based on NCG_{Zn} (The mass ratio of GO/BPD was 1:10, the molar ratio of BPD/$ZnCl_2$ was 1:0.6, and the pyrolysis temperature was 650℃.): (a) Cyclic voltammetry curves at different scan rates (1-20 mV s^{-1}). (b) Galvanostatic charge/discharge curves at different current densities (0.5-20 A g^{-1}).

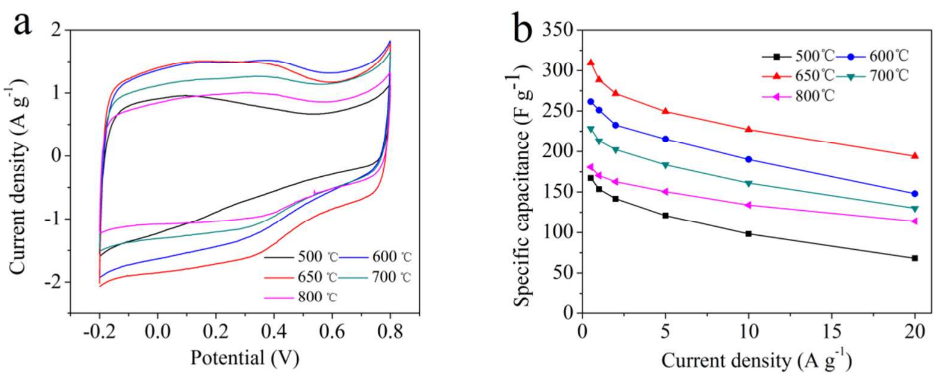

Figure S13. Electrochemical characterization of supercapacitors based on NCG_{Zn} samples with different pyrolysis temperature (500, 600, 650, 700 and 800 ℃, respectively): (a) Cyclic voltammetry curves at a scan rates of 5 mV s^{-1}. (b) The specific capacitances at different current density ranging from 0.5 to 20 A g^{-1}.

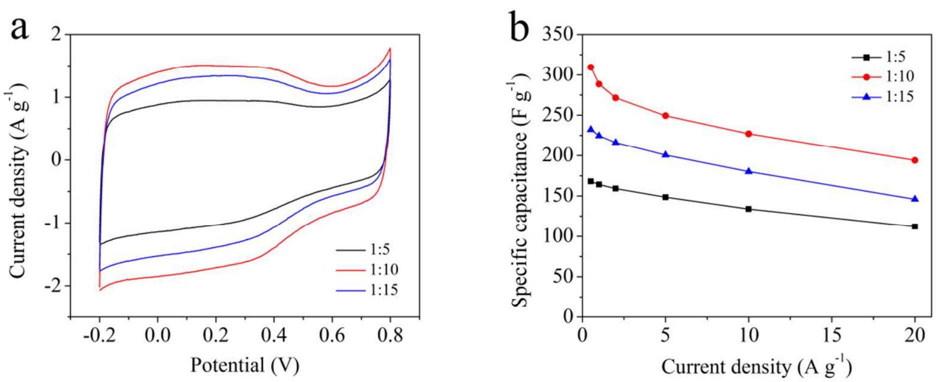

Figure S14. Electrochemical characterization of supercapacitors based on NCG_{Zn} samples with different mass ratio of GO/BPD (1:5, 1:10 and 1:15, respectively): (a) Cyclic voltammetry curves at a scan rates of 5 mV s^{-1}. (b) The specific capacitances at different current density ranging from 0.5 to 20 A g^{-1}.

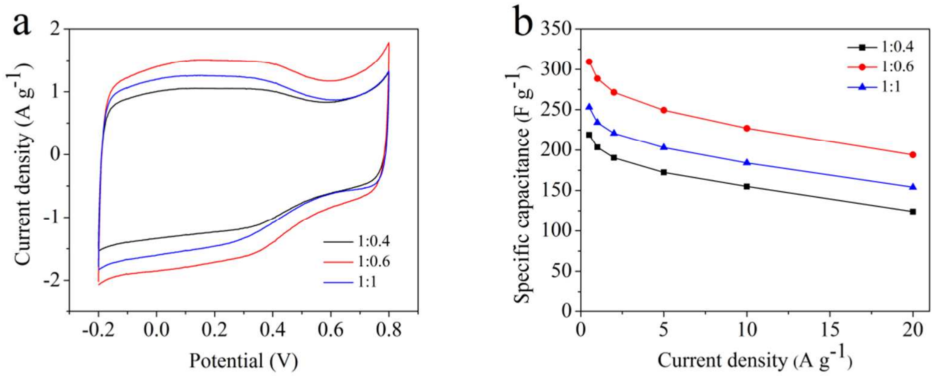

Figure S15. Electrochemical characterization of supercapacitors based on NCG_{Zn} samples with different molar ratio of BPD/$ZnCl_2$ (1:0.4, 1:0.6 and 1:1, respectively): (a) Cyclic voltammetry curves at a scan rates of 5 mV s^{-1}. (b) The specific capacitances at different current density ranging from 0.5 to 20 A g^{-1}.

7. The comparison of electrochemical properties of the reported materials and the present work.

Table S6. The comparison of gravimetric specific capacitances of the reported N-doped carbons or nitrogen-doped graphene/carbon composite materials and the present work

Samples	C (F g^{-1})	Ref
3D hierarchical porous carbon fibers	329 (0.1 A g^{-1})	1
Activated polyaniline-based carbon nanoparticles	331 (0.2 A g^{-1})	2
Hierarchical porous and N-doped carbon nanotubes	365.9 (0.1 A g^{-1})	3
3D hierarchical porous carbon	318.2 (0.5 A g^{-1})	4
Biomass-derived nitrogen-doped porous carbon	320 (0.5 A g^{-1})	5
Hierarchical nitrogen-doped porous carbon	239 (5 mV s^{-1})	6

Graphitized nanoporous carbons	238 (20 mV s^{-1})	7
Porous carbons	272 (5 mV s^{-1})	8
Porous carbons	214 (5 mV s^{-1})	9
Porous carbons	211 (10 mV s^{-1})	10
Hollow, spherical nitrogen-rich porous carbon shells	230 (0.5 A g^{-1})	11
Heavily nitrogenated graphene oxide	320 (0.3 A g^{-1})	12
Graphene-incorporated nitrogen-rich carbon composite	300 (0.1 A g^{-1})	13
Graphene/nitrogen-doped ordered mesoporous carbon nanosheet	377 (0.2 A g^{-1})	14
Hierarchical porous N-doped sandwich-type carbon composites	340 (0.5 A g^{-1})	15
Nitrogen-doped carbon decorated graphene	289 (0.2 A g^{-1})	16
Three-dimensional nitrogen-doped hierarchical porous carbon/graphene	318 (1 A g^{-1})	17
N-doped activated composite	267 (5 mV s^{-1})	18
Porous nitrogen-doped graphene/carbon nanotubes composite	246.6 (0.5 A g^{-1})	19
Sandwich-like nitrogen-enriched porous carbon/graphene composites	381.6 (0.1 A g^{-1})	20
NCG_{Cu}	369 (0.5 A g^{-1})	This work
NCG_{Fe}	298.5 (0.5 A g^{-1})	This work
NCG_{Zn}	309.5 (0.5 A g^{-1})	This work

Table S7. The comparison of volumetric specific capacitances of the reported carbon materials and the present work

Samples	C (F cm^{-3})	Ref
Densely packed graphene nanomesh-carbon nanotube hybrid film	331 (5 mV s^{-1})	21
Liquid-mediated dense integration of graphene materials	261.3 (0.5 A g^{-1})	22
Compactly interlinked graphene nanosheets	376 (0.1 A g^{-1})	23
High density reduced graphite oxide	255 (1 A g^{-1})	24
Free-standing boron and oxygen co-doped carbon nanofiber films	179.3 (1 A g^{-1})	25
Sandwiched graphene/porous carbon layers	212 (0.5 A g^{-1})	26
Porous layer-stacking carbon	360 (0.5 A g^{-1})	27
Crumpled nitrogen-doped graphene	98 (1 A g^{-1})	28
Nitrogen-doped sandwich-like porous carbon nanosheets	287 (2 mV s^{-1})	29
Oxygen- and nitrogen-enriched 3D porous carbon	360 (0.5 A g^{-1})	30
Functionalized porous carbon	468 (0.5 A g^{-1})	31
NCG_{Cu}	560.9 (0.5 A g^{-1})	This work
NCG_{Fe}	278.2 (0.5 A g^{-1})	This work
NCG_{Zn}	355.9 (0.5 A g^{-1})	This work

References

(1) Li, Y.; Lu, C.; Zhang, S.; Su, F.-Y.; Shen, W.; Zhou, P.; Ma, C. Nitrogen- and Oxygen-Enriched 3D Hierarchical Porous Carbon Fibers: Synthesis and Superior Supercapacity. *J. Mater. Chem. A* **2015**, *3*, 14817-14825.

(2) Zhou, J.; Zhu, T.; Xing, W.; Li, Z.; Shen H.; Zhuo, S. Activated Polyaniline-Based Carbon Nanoparticles for High Performance Supercapacitors. *Electrochim. Acta* **2015**, *160*, 152-159.

(3) Zhu, T.; Zhou, J.; Li, Z.; Li, S.; Si, W.; Zhuo, S. Hierarchical Porous and N-doped Carbon Nanotubes Derived from Polyaniline for Electrode Materials in Supercapacitors. *J. Mater. Chem. A* **2014**, *2*, 12545-12551.

(4) Qie, L.; Chen, W.; Xu, H.; Xiong, X.; Jiang, Y.; Zou, F.; Hu, X.; Xin, Y.; Zhang, Z.; Huang, Y. Synthesis of Functionalized 3D Hierarchical Porous Carbon for High-Performance Supercapacitors. *Energy Environ. Sci.* **2013**, *6*, 2497-2504.

(5) Wei, T.; Wei, X.; Gao, Y.; Li, H. Large Scale Production of Biomass-Derived Nitrogen-Doped Porous Carbon Materials for Supercapacitors. *Electrochim. Acta* **2015**, *169*, 186-194.

(6) Jeon, J.-W.; Sharma, R.; Meduri, P.; Arey, B. W.; Schaef, H. T.; Lutkenhaus, J. L.; Lemmon, J. P.; Thallapally, P. K.; Nandasiri, M. I.; McGrail, B. P.; Nune, S. K. *In Situ* One-Step Synthesis of Hierarchical Nitrogen-Doped Porous Carbon for High-Performance Supercapacitors. *ACS Appl. Mater. Interfaces* **2014**, *6*, 7214-7222.

(7) Torad, N. L.; Salunkhe, R. R.; Li, Y.; Hamoudi, H.; Imura, M.; Sakka, Y.; Hu,

C.-C.; Yamauchi, Y. Electric Double-Layer Capacitors Based on Highly Graphitized Nanoporous Carbons Derived from ZIF-67. *Chem. Eur. J.* **2014**, 20, 7895-7900.

(8) Salunkhe, R. R.; Tang, J.; Kamachi, Y.; Nakato, T.; Kim, J. H.; Yamauchi, Y. Asymmetric Supercapacitors Using 3D Nanoporous Carbon and Cobalt Oxide Electrodes Synthesized from a Single Metal-Organic Framework. *ACS Nano* **2015**, *9*, 6288-6296.

(9) Chaikittisilp, W.; Hu, M.; Wang, H.; Huang, H.-S.; Fujita, T.; Wu, K. C.-W.; Chen, L.-C.; Yamauchi, Y.; Ariga, K. Nanoporous Carbons through Direct Carbonization of a Zeolitic Imidazolate Framework for Supercapacitor Electrodes. *Chem. Commun.* **2012**, *48*, 7259-7261.

(10) Amali, A. J.; Sun, J.-K.; Xu, Q. From Assembled Metal-Organic Framework Nanoparticles to Hierarchically Porous Carbon for Electrochemical Energy Storage. *Chem. Commun.* **2014**, *50*, 1519-1522.

(11) Liu, X.; Zhou, L.; Zhao, Y.; Bian; L.; Feng, X; Pu, Q. Hollow, Spherical Nitrogen-Rich Porous Carbon Shells Obtained from a Porous Organic Framework for the Supercapacitor. *ACS Appl. Mater. Interfaces* **2013**, 5, 10280-10287.

(12) Gopalakrishnan, K.; Govindaraj, A.; Rao, C. N. R. Extraordinary Supercapacitor Performance of Heavily Nitrogenated Graphene Oxide Obtained by Microwave Synthesis. *J. Mater. Chem. A* **2013**, *1*, 7563-7565.

(13) Fan, X.; Yu, C.; Yang, J.; Ling, Z.; Qiu, J. Hydrothermal Synthesis and Activation

of Graphene-Incorporated Nitrogen-Rich Carbon Composite for High-Performance Supercapacitors. *Carbon* **2014**, *70*, 130-141.

(14) Song, Y.; Yang, J.; Wang, K.; Haller, S.; Wang, Y.; Wang, C.; Xia, Y. *In-Situ* Synthesis of Graphene/Nitrogen-Doped Ordered Mesoporous Carbon Nanosheet for Supercapacitor Application. *Carbon* **2016**, *96*, 955-964.

(15) Luo, H.; Liu, Z.; Chao, L.; Wu, X.; Lei, X.; Chang, Z.; Sun, X. Synthesis of Hierarchical Porous N-Doped Sandwich-Type Carbon Composites as High-Performance Supercapacitor Electrodes. *J. Mater. Chem. A* **2015**, *3*, 3667-3675.

(16) Li, M.; Xue, J. Integrated Synthesis of Nitrogen-Doped Mesoporous Carbon from Melamine Resins with Superior Performance in Supercapacitors. *J. Phys. Chem. C* **2014**, *118*, 2507-2517.

(17) Yin, Y.; Li, R.; Li, Z.; Liu, J.; Gu, Z.; Wang, G. A Facile Self-Template Strategy to Fabricate Three-Dimensional Nitrogen-Doped Hierarchical Porous Carbon/Graphene for Conductive Agent-Free Supercapacitors with Excellent Electrochemical Performance. *Electrochim. Acta* **2014**, *125*, 330-337.

(18) Gharehkhani, S.; Shirazi, S. F. S.; Jahromi, S. P.; Sookhakian, M.; Baradaran, S.; Yarmand, H.; Oshkour, A. A.; Kazia, S. N.; Basirunde, W. J. Spongy Nitrogen-Doped Activated Carbonaceous Hybrid Derived from Biomass Material/Graphene Oxide for Supercapacitor Electrodes. *RSC Adv.* **2015**, *5*, 40505-40513.

(19) Lin, T.-T.; Lai, W.-H.; Lü, Q.-F.; Yu, Y. Porous Nitrogen-Doped

Graphene/Carbon Nanotubes Composite with an Enhanced Supercapacitor Performance. *Electrochim. Acta* **2015**, *178*, 517-524.

(20) Xie, Q.; Zhou, S.; Zheng, A.; Xie, C.; Yin, C.; Wu, S.; Zhang, Y.; Zhao, P. Sandwich-Like Nitrogen-Enriched Porous Carbon/Graphene Composites as Electrodes for Aqueous Symmetric Supercapacitors with High Energy Density. *Electrochim. Acta* **2016**, *189*, 22-31.

(21) Jiang, L.; Sheng, L.; Long, C.; Fan, Z. Densely Packed Graphene Nanomesh-Carbon Nanotube Hybrid Film for Ultra-High Volumetric Performance Supercapacitors. *Nano Energy* **2015**, *11*, 471-480.

(22) Yang, X.; Cheng, C.; Wang, Y.; Qiu, L.; Li, D. Liquid-Mediated Dense Integration of Graphene Materials for Compact Capacitive Energy Storage. *Science* **2013**, *341*, 534-537.

(23) Tao, Y.; Xie, X.; Lv, W.; Tang, D.-M.; Kong, D.; Huang, Z.; Nishihara, H.; Ishii, T.; Li, B.; Golberg, D.; Kang, F.; Kyotani, T.; Yang, Q. -H. Towards Ultrahigh Volumetric Capacitance: Graphene Derived Highly Dense but Porous Carbons for Supercapacitors. *Sci. Rep.* **2013**, *3*, 2975.

(24) Li, Y.; Zhao, D. Preparation of Reduced Graphite Oxide with High Volumetric Capacitance in Supercapacitors. *Chem. Commun.* **2015**, *51*, 5598-5601.

(25) Yu, Z.-Y.; Chen, L.-F.; Song, L.-T.; Zhu, Y.-W.; Ji, H.-X.; Yu, S.-H. Free-Standing Boron and Oxygen Co-Doped Carbon Nanofiber Films for Large Volumetric Capacitance and High Rate Capability Supercapacitors. *Nano Energy* **2015**, *15*, 235-243.

(26) Yan, J.; Wang, Q.; Lin, C.; Wei, T.; Fan, Z. Interconnected Frameworks with a Sandwiched Porous Carbon Layer/Graphene Hybrids for Supercapacitors with High Gravimetric and Volumetric Performances. *Adv. Energy Mater.* **2014**, *4*, 1400500.

(27) Long, C.; Chen, X.; Jiang, L.; Zhi, L.; Fan, Z. Porous Layer-Stacking Carbon Derived from In-Built Template in Biomass for High Volumetric Performance Supercapacitors. *Nano Energy* **2015**, *12*, 141-151.

(28) Wang, J.; Ding, B.; Xu, Y.; Shen, L.; Dou, H.; Zhang, X. Crumpled Nitrogen-Doped Graphene for Supercapacitors with High Gravimetric and Volumetric Performances. *ACS Appl. Mater. Interfaces* **2015**, *7*, 22284-22291.

(29) Wang, Q.; Yan, J.; Fan, Z. Nitrogen-Doped Sandwich-Like Porous Carbon Nanosheets for High Volumetric Performance Supercapacitors. *Electrochim. Acta* **2014**, *146*, 548-555.

(30) Li, J.; Liu, K.; Gao, X.; Yao, B.; Huo, K.; Cheng, Y.; Cheng, X.; Chen, D.; Wang, B.; Sun, W.; Ding, D.; Liu, M.; Huang, L. Oxygen- and Nitrogen-Enriched 3D Porous Carbon for Supercapacitors of High Volumetric Capacity. *ACS Appl. Mater. Interfaces* **2015**, *7*, 24622-24628.

(31) Long, C.; Jiang, L.; Wu, X.; Jiang, Y.; Yang, D.; Wang, C.; Wei, T.; Fan, Z. Facile Synthesis of Functionalized Porous Carbon with Three-Dimensional Interconnected Pore Structure for High Volumetric Performance Supercapacitors. *Carbon* **2015**, *93*, 412-420.